University of Amsterdam

Master thesis

Particle based 3D modeling of positive streamer inception

Author:
Jannis Teunissen

Supervisor:
Prof. Ute Ebert

November 6, 2011

Abstract

In this report we present a particle based 3D model for the study of streamer inception near positive electrodes in air. The particle code is of the PIC-MCC type and an electrode is included using the charge simulation method. An algorithm for the adaptive creation of super-particles is introduced, that keeps single electrons in regions of low density. Photoionization is included as the source of secondary electrons. We discuss the model implementation and present results on avalanche statistics and the inception process in general. Although the inclusion of the electrode is currently still somewhat inaccurate, the model seems to be a powerful tool with which one is able to study the full physics of the first few nanoseconds of a discharge. We present simulation results that show good agreement with experimental observations: first an initiation cloud forms around the electrode tip, which later starts to destabilize into streamers.

Contents

I. INTRODUCTION

Recent years have seen an active development of several plasma discharge applications such as pollution control [1], ozone generation [2], wound sterilization [3] or the treatment of biogases [4]. Discharges occur when a dielectric that is exposed to a large voltage difference starts to become conducting, which is sometimes also referred to as electrical breakdown. Most discharges start from electron avalanches, that can form when the electric field (due the voltage difference) exceeds the 'breakdown field'. The formation of such avalanches begins with a 'free' electron, that can for example appear due to background radiation. Under the influence of the electric field it accelerates and gains energy, but while moving it will have collisions with the neutral atoms or molecules, in which the electron is scattered and loses some energy. In a higher electric field the electron will have a higher energy, on average. Above the breakdown field the probability of ionizing a neutral through impact ionization becomes larger than the probability that the electron is removed due to some loss mechanism. An additional free electron created in an ionization can itself ionize other neutrals, and so an electron avalanche may form that grows rapidly in size. From these avalanches different types of discharges can form, some of which are listed in table I, for example the glow and arc discharge that are stationary, or the streamer and leader formation that are transient.

Here we focus on streamers that play an important role in nature, as they prepare the path of lightning leaders and seem to generate X-ray radiation [6]. Streamers are thin conducting plasma channels surrounded by a space charge layer that propagate at a high velocity, typically 10^5 up to 10^7 m/s in air. They are in most cases formed in a region where the electric field is above the breakdown value, but can propagate to regions where the electric field is much lower. This is possible because the strongly curved front of a streamer enhances the field ahead of it.

Streamers can propagate in the direction of the electric field (positive streamers) or against it (negative streamers), see figure 1. In both cases impact ionization by energetic electrons in front of the streamer is the main mechanism of extending the plasma channel, but while for negative streamers these electrons can just come from the channel itself, for positive streamers a source of electrons ahead of them is required.

In this report we study the inception of streamers in air near a positive electrode with a sharp tip. Experimental observations have provided more insight into this process, as will be discussed in section II. Often a so-called initiation cloud is formed around the electrode tip, which grows up to some radius but then destabilizes into one or more streamers. Several fundamental questions arise, e.g., it is unclear what controls the formation and consecutive destabilization of the initiation cloud and how this influences the shape and velocity of the resulting streamers.

To help answer these questions we have developed a particle based 3D simulation to study the inception of discharges near positive electrodes. Arguments for the choice of model and a description of the implementation are given in section III and IV, where also the general difficulties in the modeling of this type of discharge are discussed. In section V the simulation results are presented. We discuss the accuracy of our model and address some of the main challenges of this research:

- To understand the conditions and the stochastic delay of inception.
- To understand the formation and destabilization of the initiation cloud, and how this determines the streamer diameter and velocity.
- To obtain the charge density and electron energy distribution during the inception process.

To our knowledge, this is the first particle model that can be used for the study of inception near positive electrodes. We make several suggestions for improvements in section VI, and conclude with a summary of our results in section VII.

II. POSITIVE STREAMER INCEPTION

The inception of positive streamers near a positive electrode starts with an initial electron avalanche moving towards the electrode. When the avalanche reaches the electrode, the electrons will be absorbed, leaving behind positive ions (that move much slower in the opposite direction). To sustain this process new 'seed' electrons have to be created to

	Without space charge	With space charge	With heating
Transient	avalanche	streamer	leader
Stationary	Townsend	glow	arc / spark

TABLE I: Characterization of stationary and transient discharges from [5], based on whether they are significantly influenced by space charge or heating.

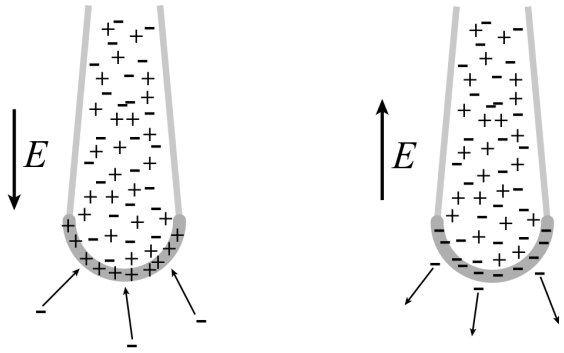

FIG. 1: Picture taken from [5], showing a positive (on the left) and negative (on the right) streamer moving downwards. The plus symbols indicate positive ions while the minus symbols indicate free electrons.

form consecutive avalanches. Such electrons can be created by volume photoionization or detachment, or they could be emitted from a negative electrode if there is one nearby (due to field emission, ion impact or the photo-electric effect). We only consider photoionization in this work.

Above some critical voltage V_c the number of electrons and ions starts to grow rapidly. Positive ions concentrate near the electrode, left behind by the electrons that are absorbed by the electrode, extending the positive potential outwards. Many different shapes of discharges can form. If the voltage is relatively low and the electrode sharp, the build up of space charge will 'round off' the electrode, leading to a weaker electric field. Therefore a stable state can be reached, as the weaker electric field prevents further growth. If the electrode voltage is increased further the space charge around the electrode grows, forming an ionized cloud around the tip. At some point small perturbations in the cloud can start to grow because they enhance the local electric field, and the cloud destabilizes into one or more streamers (therefore it is referred to as initiation cloud or inception cloud).

The critical voltage V_c depends on the electrode geometry, but also on the pressure, the temperature and the gas composition. Because electron-neutral collisions (e.g., ionization, excitations, attachment) dominate the behavior of streamers, properties of streamers often scale in a simple way with the density of the neutrals [7]. Typical scales are: an electric field of $10^7\ (N/N_0)$ V/m, where N is the number density of the neutrals and $N_0 = 2.5 \cdot 10^{25}\ \mathrm{m}^{-3}$ is the number density of air at 1 bar and 293 K, an 'ionization length' (the distance between ionizations caused by an electron) of $10^{-6}\ (N_0/N)$ m, a velocity of 10^6 m/s and an electron density of $10^{20}\ (N/N_0)^2\ \mathrm{m}^{-3}$. The typical length scale for photoionization is about $5 \cdot 10^{-4}\,(N_0/N)$ m in air, see section IV E. The breakdown electric field, above which electron avalanches can form, is approximately $3 \cdot 10^6$ V/m in air at 1 bar (and does not scale in a simple way, because it depends on the rate of three-body attachment).

Time-resolved photographs of the streamer inception process in air and other gases have been taken by Briels et al. [8, 9], and later by Nijdam et al. [10, 11]. Figure 2 shows that first a initiation cloud forms that later destabilizes into streamers; different pressures and voltages are imaged. These and other experimental observations have provided more insight into the formation of streamers, but at the same time they have also raised fundamental questions about the governing mechanisms of the inception process. It is currently not understood what controls the size and shape of the initiation cloud and when it starts to destabilize. There is also little knowledge about the electron energy distribution during the inception which influences the generation of excited molecules and is therefore important for many applications.

III. SIMULATION MODEL

There are several approaches to modeling low temperature discharges. Particle models track individual or groups of particles and are usually of the PIC-MCC (particle in cell, Monte Carlo collision) type [12–14]. As this is the most direct type of modeling, particle methods can capture the full physics of a discharge. Fluid models on the other hand work with densities and are often of the 'drift-diffusion-reaction' type [15]. Such models are typically based on the local field approximation, which assumes that the plasma is relaxed to the local electric field, and they contain no direct information about the electron distribution function. There are also kinetic models, which solve the Boltzmann equation (in some approximate form) [16]. They in principle contain the electron energy distribution, allowing them to capture most of the physics of a discharge. Different approaches can also be combined to form hybrid models, where, for example, a fluid model is used for the interior region of a plasma and a particle model for the exterior region [17].

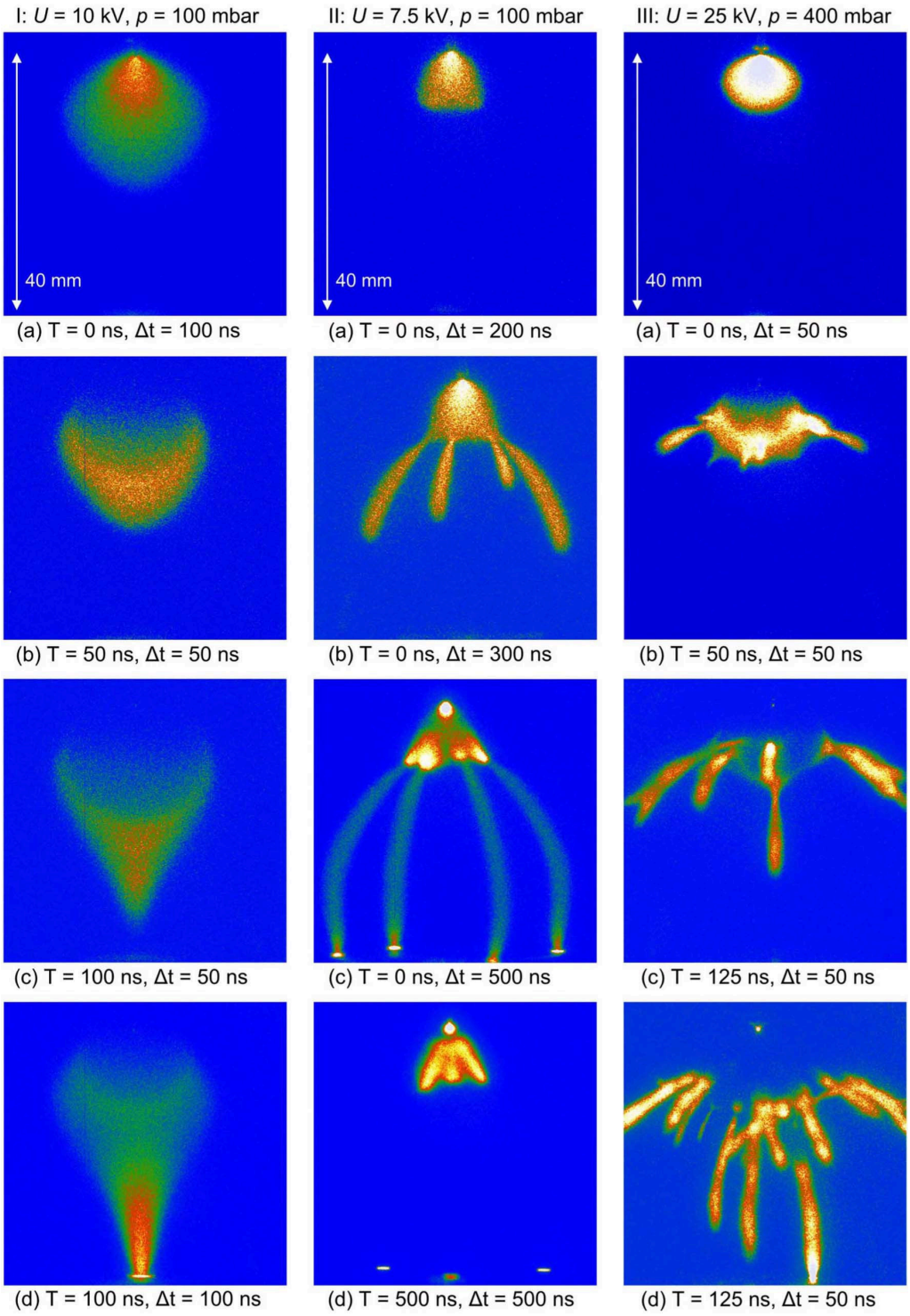

FIG. 2: Picture taken from [8] showing time resolved photographs of the evolution of a positive discharge in air for different pressures and voltages. The electrode at the top is sharp and the bottom electrode is planar, with a distance of 40 mm between them. The exposure time is indicated by Δt and starts at T. According to discharge similarity laws a length scale of 40 mm at 100 mbar corresponds to 4 mm at 1 bar [9].

Accurate modeling of discharges has proven to be challenging; the strong gradients in density and electric field require a fine spatial resolution, which is the reason that most density based simulations are performed in 2D. On the other hand the large number of charged particles (at normal pressure typically above 10^8 during inception, and increasing further) limits the usage of particle based models to the early stages of the discharge.

Our interest lies in simulating the inception of discharges near positive electrodes, and we have chosen to develop a PIC-MCC code for this purpose. There are several arguments to work with a particle code instead of the popular drift-diffusion-reaction type codes: it is not clear how good the local field approximation will be near a sharp electrode, the inception process should be simulated in 3D and important stochastic fluctuations (e.g., the probabilistic presence of a few electrons) cannot be modeled with a density approximation. Furthermore, the particle models are almost fully based on first principles allowing for a more direct comparison with experiments.

Accurate kinetic models are rather complicated to implement for such experiments, whereas the relative simplicity of PIC-MCC codes leaves them as a natural choice.

A. The PIC-MCC method

Directly computing the Coulomb interaction between N particles takes $O(N^2)$ time, which makes it infeasible for large N. Particle-in-cell methods (also known as particle-mesh methods) resolve this basic problem in modeling by mapping particles to charge densities on a grid and then computing the resulting electric field on that grid, in which the particles move until the next timestep. Close range interaction are not accounted for correctly in this way, but these often do not contribute significantly to the macroscopic behavior that one wants to study. For example, in a typical discharge plasma with an electron density of $10^{20}\,\mathrm{m}^{-3}$, the average distance between electrons is about 200 nm. The electric field of an elementary charge at this separation is only about 1% of the breakdown electric field, while the external field is often much higher, which justifies not resolving the close range interactions accurately. (If they need to be resolved there are also $\mathrm{P}^3\mathrm{M}$ methods, which combine a direct method with a particle-mesh method [18].)

A discharge forms a collision-dominated, reactive plasma, where electron-neutral collisions dominate the behavior. Important processes are for example impact ionization, (in)elastic scattering and electron attachment. With a MCC (Monte Carlo collision) scheme the time and type of these collisions are determined by Monte Carlo methods. An overview of the history of PIC-MCC modeling can be found in [12].

IV. IMPLEMENTATION

The simulation was implemented in the FORTRAN 90 programming language, building on earlier work by C. Li [17], who developed a hybrid particle-fluid model for streamer simulations. Let us discuss briefly what is simulated before going into a detailed description of the different components of the model. The model tracks electrons as particles, and ions as densities on a grid. Neutral gas molecules are not simulated, instead they provide a background of constant density. Excited molecules are not tracked either, but to include photoionization photo-emitting excited molecules are represented as a density on a grid. The simulations are intended to run for a short time (up to a few nanoseconds) and the gas is assumed to be weakly ionized, so that heating, recombination and multi-step excitations or ionizations can be neglected.

A. Electric field and electrode

Although a classical problem, computing the electric field in the presence of space charge and electrodes still proves to be challenging, because it needs to be done fast and accurately at each timestep. Without an electrode the typical strategy would be to first determine the charge density on a grid, then compute the potential by solving Poisson's equation (with some boundary condition), from which finally the electric field can be found.

The choice of grid and solver for the Poisson problem largely determines how an electrode can be included in the domain. With a finite element method one can impose part of the boundary of the domain on the electrode, whereas an embedded boundary method could be used for iterative solvers on rectangular grids. Another approach that works for any grid and solver is to use the charge simulation method (CSM).

Although finite element methods are quite flexible with regard to different geometries of the domain and electrode, they are rather difficult to implement and it is hard to judge their performance in advance, especially since the moving streamer boundary needs to be resolved accurately. On the other hand embedded boundary methods for the Poisson equation [19] look promising and have been successfully implemented for streamer simulations in 2D (see [20] which also contains some further comments on other techniques). As we are currently still exploring possible

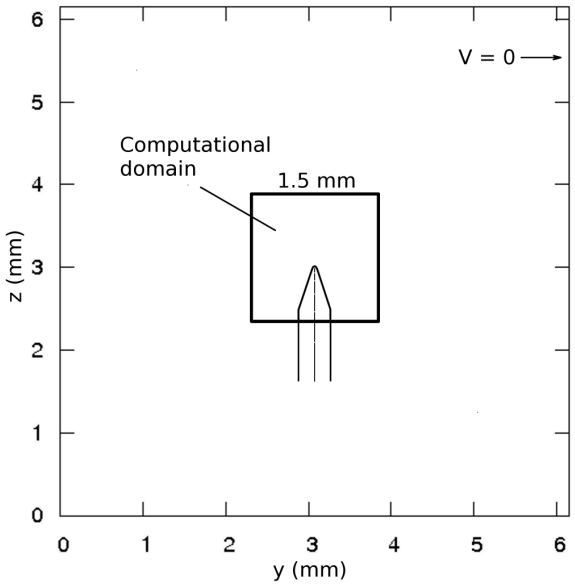

FIG. 3: Slice through the computational domain with the electrode. Both are embedded in a larger region that is used to compute the potential at the boundary of the computational domain. Also shown are a few line charges on the axis of the electrode.

implementations of such a solver in 3D, we have opted for a simpler approach using the charge simulation method in this project, although this leads to some severe limitations as will be discussed below.

A first attempt to perform discharge simulations with the charge simulation method was made by C. Li [21], that we have now extended further. With this method (also known as the capacity matrix method [18]) one places fictitious charges on the inside of conductors, with the charges chosen such that they give approximately the right potential on the boundary of the conductor, see for example [22]. A set of control points that lie on the surface of the electrode is generated and kept during the simulation. We place line charges on the axis of the electrode, with shorter line segments towards the tip. Then the potential in the domain due to only the space charge is computed, and each control point gets the value $V_{\text{elec}} - V_{\text{space charge}}$, where V_{elec} is the electrode voltage and $V_{\text{space charge}}$ the electric potential due to the space charge. As the effect of a line charge λ_i on the potential at a control point is linear in λ_i one can now solve a linear system to obtain the 'best' approximation to V_{elec} at the control points. If there are more control points than line charges, the system is over-determined and one seeks the least-squares solution. We place 200 control points on the electrode surface that are evenly spread along the axial direction of the electrode, but each at a random orientation. The length of the line charges l_i is chosen as

$$l_i = L_{\text{elec}} \left[\left(\frac{i+1}{N_l} \right)^s - \left(\frac{i}{N_l} \right)^s \right], \tag{1}$$

where N_l is the number of line charges, L_{elec} the length of the electrode and s a real number. The first line charge lies a distance $L_{\text{elec}} \cdot (1/N_l)^s$ from the electrode tip, and the consecutive line charges are placed without leaving gaps. When the positions of the control points and of the line charges are known, the least squares solution of the linear system can be found. We initially try multiple values for s from the interval [0.5, 4] and select the one that leads to the lowest maximum error (at the control points) times the square root of the condition number of the linear system. If the maximum error at the control points has doubled during the simulation, we change the value of s with the same procedure.

For the computation of the potential due to space charge a Cartesian grid of size M_x, M_y, M_z is used, representing a physical volume of size $L_x \times L_y \times L_z$. From figure 2 we can see that a region of at least $(1\,\text{mm})^3$ should be modeled to capture the inception process at normal pressure. At the same time we want to limit the number of grid cells to a few million (so that a simulation can be done in about a day), and therefore we use $(128)^3$ cells of size $(12\,\mu\text{m})^3$, representing a total volume of about $(1.5\,\text{mm})^3$. Electrons and ions are mapped to charge densities using trilinear interpolation, a common choice known as cloud-in-cell or CIC [14]. For ions this occurs only when they are created, as they are stored on a grid with the accumulated ion density. The ion density flows by drift and diffusion, see section IV B. For the electrons, that are tracked as particles, the charge density is recomputed at each timestep.

The 'free' region around the electrode (i.e., where there are no physical boundaries) in experiments performed by Briels et al. [8, 9], and Nijdam et al. [10, 11] is of the order of centimeters. Because our computational domain is much

smaller we determine the potential at its boundary in the following way. First the potential from the space charge is solved on a coarser grid, representing a 4^3 times larger volume, with a Dirichlet boundary condition $V_{\mathrm{bc}} = 0$, see figure 3. Then the result is interpolated back to obtain the Dirichlet boundary conditions for the smaller simulation domain. Now the potential in the simulation domain due to the space charge is computed, after which the charge simulation method is used to find the λ_i at the electrode axis. Finally the potential is recomputed, but now including the electrode charges and their effect on the boundary (which is found from an analytical formula for the potential of a line charge).

To solve Poisson's equation (i.e., compute the potential) we use the FISHPACK [23] solver, which is based on cyclic reduction and the fast Fourier transform. It runs approximately in time $O(n_G \log n_G)$, with n_G the number of grid cells. The electric field in the x-direction is computed as $E_{x,i,j,k} = (V_{i+1,j,k} - V_{i-1,j,k})/(2\Delta x)$, with similar expressions for the y and z-direction.

There are some severe problems with the approach described above. In the charge simulation method the least squares solution of a linear system is used, and such a solution can be influenced more strongly by a change in the surrounding space charge than is physically realistic. The simulated charges on the axis can even undergo a discontinuous jump to a different configuration, leading to a large change in the electric field. Furthermore, setting up the charges on the axis so that the electrode is well-represented and so that the linear system is not too ill-conditioned, is something that can usually only be done by hand.

These disadvantages are quite severe, and therefore we are actively looking for other methods to compute the electric field with an electrode, see section VI. On the other hand it should be noted that in experiments the voltage on the electrode over time is often also far from smooth, see for example [10].

A more general problem is that we want to simulate an electrode with a sharp tip. For a completely sharp tip the electric field diverges at the tip, which illustrates that accurate solutions are hard to obtain with almost any numerical method. When the tip is rounded there is no divergence, but accurately describing the rapidly increasing electric field towards the tip requires a very fine mesh.

B. Particle mover

The particle mover implements the following scheme to update the particles' position $\mathbf{x}$ and velocity $\mathbf{v}$ over time

$$\begin{aligned} \mathbf{x}(t + \Delta t) &= \mathbf{x}(t) + \mathbf{v}(t)\Delta t + \tfrac{1}{2}\mathbf{a}(t)\Delta t^2, \\ \mathbf{v}(t + \Delta t) &= \mathbf{v}(t) + \tfrac{1}{2}\left[\mathbf{a}(t) + \mathbf{a}(t + \Delta t)\right]\Delta t, \end{aligned} \tag{2}$$

where $\mathbf{a}(t)$ is the acceleration of the particle due to external forces. Because we assume to work under electrostatic conditions without an external magnetic field, $\mathbf{a}(t)$ is proportional to the electric field and does not depend on $\mathbf{v}(t)$. Therefore the scheme is explicit, and it can be seen to be second order accurate.

The above equations, known as the 'Velocity Verlet' algorithm [24], are very similar to a leapfrog scheme but have the advantage that the position, velocity and acceleration of a particle are defined at the same moment in time. This also simplifies the computation of the position and velocity between timesteps, relevant for collision processes.

Since the particles can have very different velocities, there is no single timestep for the movement of all particles. Instead a particle i gets the following timestep

$$\Delta t_i = \Delta t / \left(1 + \left\lfloor \frac{v_i}{\bar{v}} \right\rfloor\right), \tag{3}$$

where Δt is the total timestep, v_i is the particles' velocity and $\bar{v}$ the mean velocity of all particles.

Because the ions are much heavier than electrons they move much slower. Therefore, it is often assumed that the ions do not move at all in simulations that run up to a few nanoseconds. However, with an electrode there will be a very high concentration of positive ions in the strong electric field around the electrode tip. This means both ion drift and diffusion are larger than in similar discharges without the sharp electrode. To be able to test whether the inclusion of ion movement is important, we have implemented a first-order scheme for drift and diffusion. In this scheme we use a constant mobility and diffusion coefficient for all ions, given by $\mu = 5.0 \cdot 10^{-4}$ m^2/(Vs) and $D_c = 5.0 \cdot 10^{-4}$ m^2/s (which are rather high, see [25]). From our simulations it seems that ion movement is important close the electrode, where there is a strong electric field and a high ion density, but this should be investigated further.

C. Collision scheme

We include the following types of collisions from the SIGLO database [26]: elastic scattering, excitations, attachment and ionization. Electron-ion collisions are not considered because at a low degree of ionization they rarely occur, and

recombination is not included because we simulate only up to a few nanoseconds (see [27]).

In our Monte Carlo collision scheme the probability of a collision i occurring in a time $dt \to 0$ is given by $\lambda_i(t)dt$, where $\lambda_i(t)$ expresses the collision rate:

$$\lambda_i(t) = N_0\, v(t)\, \sigma_i(v), \tag{4}$$

with N_0 the number density of neutral molecules (assumed to be constant), $v(t)$ the velocity of the electron, and $\sigma_i(v)$ the total cross section for an electron with velocity v.

If the total collision rate $\lambda_{\mathrm{T}}(t) = \sum_i \lambda_i(t)$ is introduced, then the probability $P(t_0, t_1)$ of having a collision in a finite interval $[t_0, t_1]$ is given by:

$$P(t_0, t_1) = 1 - \exp\left[-\int_{t_0}^{t_1} \lambda_{\mathrm{T}}(t)\, dt\right], \tag{5}$$

and the so-called *null-collision method* [13] can be used. With this method one first applies rejection sampling to determine the next collision time, given some maximum collision rate $\lambda_{\mathrm{T,max}}$. To compute the rejection probability efficiently we approximate the integral in (5) as

$$\int_{t_0}^{t_1} \lambda_{\mathrm{T}}(t)\, dt \approx (t_1 - t_0) \cdot \lambda_{\mathrm{T}}(t_{1/2}), \tag{6}$$

with $t_{1/2} = (t_0 + t_1)/2$, so that it is second order accurate. (We would like to point out that in some PIC-MCC codes the integral is approximated only to first order, for example as $\lambda_{\mathrm{T}}(t_1)$, but this gives a systematic error even if the timestep goes to zero.) A collision type is then chosen randomly, with the probability proportional to the collision rates $\lambda_i(t)$.

We follow a similar approach as C. Li [17], Chanrion and Neubert [28] and references therein [29–32] for the implementation of the various collisions, with cross sections obtained from the SIGLO database [26]. The air in our simulations consists of 78% N_2, 21% O_2 and 1% Ar. For each gas the SIGLO database contains cross sections for elastic collisions, ionizations and different excitations (23 for N_2, 13 for O_2 and 1 for Ar), and for O_2 there are also cross sections for two- and three-body attachment. The cross sections are intended to be used with isotropic scattering, but can be transformed to use anisotropic scattering formulas, see for example [17].

For elastic collisions between electrons and N_2 molecules the formulas for anisotropic scattering from Okhrimovskyy et al. [30] are used. They use a normalized differential cross section of the form [33]

$$I(\varepsilon_h, \chi) = \frac{1}{4\pi} \frac{1 - \xi(\varepsilon_h)^2}{\left[1 - \xi(\varepsilon_h)\cos\chi\right]^2}, \tag{7}$$

where ε_h is the electron energy divided by the Hartree energy ($E_{\mathrm{h}} = 27.21$ eV), χ is the scattering angle and $\xi(\varepsilon)$ is a fitting parameter that can be derived from the ratio between the integrated and the momentum transfer cross sections. In the case of N_2 they give the following approximation

$$\xi(\epsilon) \approx \frac{0.065\epsilon + 0.26\epsilon}{1 + 0.05\epsilon + 0.2\sqrt{\epsilon}} - \frac{12\sqrt{\epsilon}}{1 + 40\sqrt{\epsilon}}, \tag{8}$$

where ϵ is the electron energy in eV. The scattering is approximately isotropic at low energies (< 5 eV) and peaked in the forward direction at high energies. For elastic scattering on other molecules (O_2, Ar) we use the formula given by Surendra et al. in [34], which leads to a similar scattering pattern:

$$I(\epsilon, \chi) = \frac{\epsilon}{4\pi \ln(1 + \epsilon)} \frac{1}{1 + \epsilon \sin(\chi/2)^2}. \tag{9}$$

where ϵ is the energy of the electron in eV. The energy of the scattered electron ϵ_{scat} in terms of the incident electron energy ϵ_{inc} is approximated to first order in m_e/M by

$$\epsilon_{\mathrm{scat}}/\epsilon_{\mathrm{inc}} = 1 - 2m_e/M \cdot (1 - \cos\chi), \tag{10}$$

where m_e is the mass of the electron and M is the mass of the neutral molecule. This can be important in noble gases, because there are no other energy loss mechanism for low energy electrons in such gases.

In an inelastic collision the electron's energy is reduced by the excitation threshold and then scattered as if it were an elastic collision (as was done in [34]). Excited molecules are not tracked in the simulation and hence interactions between electrons and these molecules are not included (like multi-step excitations or ionizations).

In an ionizing collision the energy is split between incident and newly created electron according to an empirical fit by Opal [31], see also [29]. The newly created electron gets the energy

$$\epsilon_{\text{new}} = \beta \tan\left[U \arctan\left(\frac{\epsilon_{\text{inc}} - \epsilon_\alpha}{2\beta}\right)\right], \tag{11}$$

where β is a constant with the value 13.0 eV for N_2, 17.4 eV for O_2 and 10.0 eV for Ar, U is a uniform $(0, 1]$ random number, ϵ_{inc} is the energy of the incident electron and ϵ_α the ionization potential. The energy of the scattered incident electron, ϵ_{scat} is determined by $\epsilon_{\text{scat}} + \epsilon_{\text{new}} = \epsilon_{\text{inc}} - \epsilon_\alpha$. Then the new and scattered electron are given a new direction with the same formula as for elastic scattering, with the velocity of the new electron initially in the direction of the incoming electron.

Electron attachment is implemented by simply removing the electron and subtracting one ion from the positive ion density at the electron's location.

D. Time step control

There are different timescales to consider: the time an electron can move before the variation of the electric field becomes significant, the timescale on which ion movement due to drift and diffusion is relevant and the time in which the space charge from electrons and ions has changed significantly (and thus also the resulting electric field).

In our simulations we use three different timesteps. The first one, τ_{MC}, is the Δt used in (3). It determines the maximum time a particle can move before it gets an updated value for its acceleration. The second timestep, τ_{E}, controls after how much time the electric field is recomputed from the space charge distribution, and the ion density is only advanced every τ_{ion}, the third timestep.

While $\tau_{\text{ion}} = 10^{-12}$ s is kept constant, τ_{MC} and τ_{E} are adjusted during a simulation. To control the timesteps the errors ζ_{MC} and ζ_{E} are estimated, where ζ_{MC} is found by advancing a copy of m randomly chosen particles according to (2) and then computing

$$\zeta_{\text{MC}} = \sum_{i=1}^{m} |\mathbf{a}_i(t + \Delta t) - \mathbf{a}_i(t)| \Big/ \sum_{i=1}^{m} |\mathbf{a}_i(t)| \,. \tag{12}$$

Similarly, ζ_{E} is found by comparing the electric field at the position of m randomly chosen particles before and after it has been recomputed

$$\zeta_{\text{E}} = \sum_{i=1}^{m} |\mathbf{E}_{i,\text{new}} - \mathbf{E}_{i,\text{old}}| \Big/ \sum_{i=1}^{m} |\mathbf{E}_{i,\text{old}}| \,. \tag{13}$$

Then the errors are compared with the desired errors $\zeta_{\text{MC},0}$ and $\zeta_{\text{E},0}$, and if the error is less than half the desired error, then the timesteps are increased by $(\zeta_{\text{MC},0}/\zeta_{\text{MC}})^{0.1}$ and $(\zeta_{\text{E},0}/\zeta_{\text{E}})^{0.1}$, respectively. If the error is larger than the desired error, then the timesteps are reduced by a factor of $\zeta_{\text{MC}}/\zeta_{\text{MC},0}$ and $\zeta_{\text{E}}/\zeta_{\text{E},0}$, respectively.

Because we take the global error norm the error in the electric can become larger than desired in a region where electric field changes rapidly. Ideally one would have local timesteps for different parts of the domain, but this is left for future work.

E. Photoionization

The following photoionization process is important for the development of positive streamers in air

$$N_2^* \to N_2 + \gamma,$$
$$O_2 + \gamma \to O_2^+ + e,$$

where γ is a photon with a wavelength between 98 and 102.5 nm. This process can generate free electrons around the streamer head, so that it can grow from new avalanches. The experimental data on the generation of photoelectrons is however far from conclusive, and mostly based on a single experiment [35].

We follow a similar approach as Chanrion and Neubert [28], implementing a discrete, stochastic version of the frequently used Zhelezniak model [36], see also [37]. In the traditional Zhelezniak model, the number of ionizing photons generated is proportional to the number of ionizations, with the proportionality constant depending on the

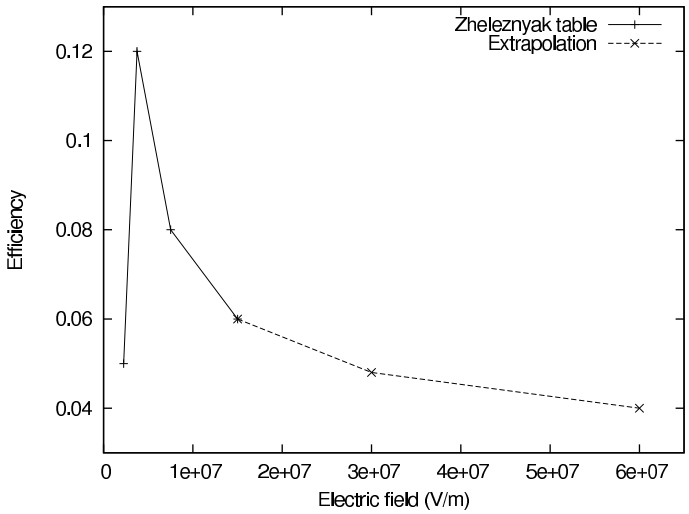

FIG. 4: The electric field dependent efficiency of photoionization [36], expressed as the number of ionizing photons generated per ionization if there would be no collisional quenching. The extrapolation is made somewhat arbitrarily.

electric field. This model works under the local field approximation and assumes a steady state, so it does not account for the delay between the generation of excited states and their decay.

It would be natural to generate such excited states for the photoionization by using the inelastic collisions of N_2, but since no authors seem to have taken such an approach before and there is a lack of data, we assume that the generation is proportional to the number of ionizations. In our simulation we use a grid (of the same size as the grids for the space charge) to which the number of ionizations occurring in a timestep are added. We assume this number is proportional to the number of photo-emitting states. After a timestep Δt on average a fraction $1 - \exp(-\Delta t/\tau_{\text{exc}})$ of the photo-emitting states would decay, with τ_{exc} the mean life time of such states, so the numbers on the grid are multiplied by this factor (to keep them proportional to the number of photo-emitting states).

We can thus also find a quantity n^*, proportional to the number of decayed states per cell. This quantity is then multiplied by a quenching factor $p_q/(p + p_q)$ with p the pressure and p_q the quenching pressure, to account for collisional quenching of the photo-emitting states (the quenching pressure is the pressure at which half of the excited states decay due to collision quenching). The expected number of photons n_{ph} is found by multiplying by $\eta^*(|\mathbf{E}|)$, representing the electric field dependent efficiency of the process, see figure 4. The actual number of created photons is finally determined by drawing a random number χ:

$$\chi \sim \text{Pois}\left(n_{\text{ph}}\right), \tag{14}$$

where $\text{Pois}(\lambda)$ is the Poisson distribution with parameter λ, and we take $p_q = 40\,\text{mbar}$ and $\tau_{\text{exc}} = 0.1\,\text{ns}$. The mean absorption length k_f of a photon depends on its frequency f, and we use the approximation given by [37, 38]

$$k_f = k_1 \cdot (k_2/k_1)^{(f-f_1)/(f_2-f_1)}, \tag{15}$$

where $f_1 = 2.925{\cdot}10^{15}\,\text{Hz}$ and $f_2 = 3.059{\cdot}10^{15}\,\text{Hz}$ are the minimum and maximum frequency of an ionizing photon, and $k_1 = 2.625{\cdot}10^3\,P_{\text{O}_2}\,\text{bar}^{-1}\,\text{m}^{-1}$ and $k_2 = 1.5{\cdot}10^5\,P_{\text{O}_2}\,\text{bar}^{-1}\,\text{m}^{-1}$ are the corresponding absorption coefficients, with P_{O_2} the partial pressure of O_2. We assume that the photon frequencies are distributed uniformly, so that $(f - f_1)/(f_2 - f_1)$ can be sampled by a $(0, 1]$ uniform random number U. The direction of the photon is assumed to be isotropically distributed, and the distance it will travel before causing an ionization is drawn from the exponential distribution as $d_{\text{photon}} = -\ln(U_1)/k_f(U_2)$, with U_1, U_2 both a $(0, 1]$ uniform random number. At the place of absorption an electron–ion pair is created, with an initial electron energy equal to the excess energy of the photon. The mean distance a photon will travel in air at normal pressure is approximately 0.44 mm. This implies that a significant fraction of the photoionizations take place outside our simulation domain of volume $(1.5\,\text{mm})^3$ (and they are therefore not included). Initially most of the 'far away' electrons would attach to O_2 before creating an avalanche, so that they can indeed be neglected. But later, when the discharge gets close to the boundary of the domain, they should be included. This is left for future work.

F. Adaptive creation of super-particles

As the number of electrons in the simulation grows rapidly during the inception process, it becomes infeasible to track all of them individually. For example, in a typical simulation the number of electrons quickly rises to 10^9. Because roughly 100 bytes of memory are required per particle (using 64 bit floating point numbers), about 100 gigabyte of memory would be required, not even taking into account the computational cost.

The usage of so called *super-particles* has historically been essential to applications of PIC-MCC methods in plasma simulations. A super-particle represents many real particles, but behaves similar as a single one, because the charge to mass ratio is the same. The usage of super-particles leads to extra 'noise', because fewer particles with each higher mass and charge give larger statistical fluctuations in macroscopic quantities than is physically realistic. However, for many applications one can still get meaningful results, with a much lower computational cost.

In our simulations the particles are electrons that, on average, move towards the positive electrode, and there are strong density gradients. This does not favor the introduction of statically weighted super-particles (all have the same weight), since the low density regions where electron avalanches are formed would be too noisy. Therefore the following adaptive rescaling algorithm for electrons is implemented.

For each cell in the domain, determine the number of particles in that cell that can be rescaled. These particles can be filtered by setting limits on their energy, super-particle-weight or acceleration. Then if a cell contains at least $M_{\min}$ candidates for rescaling, generate a list of the particles' indices, sorted by velocity from low to high. For each such cell select a pair of consecutive particles from the list. If the velocities of particles i and $i+1$ differ less than $\delta \cdot \max(\bar{v}, v_{i+1})$, where $\delta = 0.01$ is some threshold, $\bar{v}$ is the mean velocity of all the particles and v_{i+1} is the velocity of particle $i+1$, they are merged: one is marked inactive and the other gets the combined weight of the particles. The new velocity is chosen such that energy is conserved, and the direction and position of the new particle are chosen from one of the original particles (taking the average leads to a bias towards the cell centers). The choice between the two particles is made in such a way that the present total difference in space charge distribution over the cell due to the rescaling is minimized.

If the rescaling has been successful, particles $i+2$ and $i+3$ are selected for the same procedure, otherwise $i+1$ and $i+2$ are selected, until the end of the list is reached or less than $M_{\min}$ particles are left in the cell. When all the cells are rescaled, the inactive particles are removed.

Ideally, one would like to keep the electron distribution function $f(\mathbf{x}, \mathbf{v})$ unaltered due to the rescaling. The method described above does not conserve momentum, but comes quite close to keeping the charge distribution over a cell unaltered, and does conserve energy for each merged pair of particles. The error in the electric field can become a few times larger after a timestep where all particles were merged, but then decreases as the new velocities relax to the background field. We have not analyzed the possible sampling bias in the velocity distribution over the cell.

When a super-particle undergoes an ionizing collision, the newly created electron is also a super-particle with the same weight. Ionizing photons are still created individually, so that a particle of weight w on average creates w times as many photons as a single electron.

G. Parallelization

The Monte Carlo part of the simulation is parallelized using MPI, which in principle is quite simple because the different particles are essentially non-interacting except for their coupling through the electric field, which is currently still computed sequentially and then shared. In order to perform the creation of super-particles correctly, the particles are first redistributed over the different MPI tasks, such that either all or none of the particles in a grid cell are present.

V. SIMULATION RESULTS

In this section we present and analyze the results of our simulations. First the simulated electrode is introduced, which seems to be the most problematic part of the simulation, after which a comparison is made between swarm parameters generated by our model and those from BOLSIG+ [39], to test the particle code. Then the initial avalanche size distribution is obtained for avalanches starting at different distances from the electrode, which is an important first step in understanding the inception voltage and probability. Finally, results of longer simulations are presented, where an initiation cloud destabilizes into streamers, and we also discuss the nonphysical effects of super-particles.

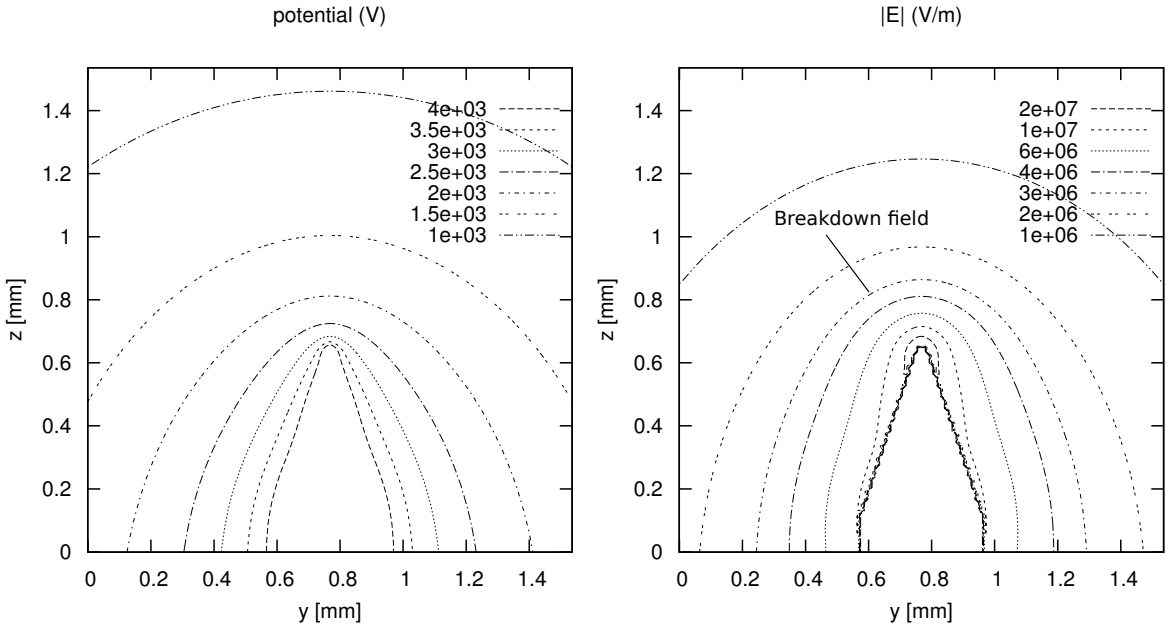

FIG. 5: Two slices through the middle of the domain, showing the potential and electric field strength around a +4.0 kV electrode without a discharge. The electrode shape is visible in the right figure, because the electric field is set to zero inside of the electrode and thus the contour lines join at the surface. Comparing with the equipotential line at 4 kV gives an idea of the accuracy of the charge simulation method, where in this case 10 line charges were used. The staircase pattern arises because only values at the cell centers are used in this plot (whereas in the simulation we define the electrode region smoothly and we use first order interpolation).

A. The electrode

The electrode shape that we use is shown in figures 3 and 5: a cylindrical base of height $h_{\mathrm{cyl}} = 1.0\,\mathrm{mm}$ and radius $r_{\mathrm{cyl}} = 0.2\,\mathrm{mm}$, with a conical tip of height $h_{\mathrm{con}} = 0.6\,\mathrm{mm}$. The tip is rounded, with a radius of curvature $\rho_{\mathrm{tip}} = 24\,\mu\mathrm{m}$, and similarly the transition between the cylindrical and conical region has radius of curvature $\rho_{\mathrm{trans}} = 50\,\mu\mathrm{m}$.

The electric field is much stronger near the tip of the electrode than at the cylindrical part, so discharges typically initiate near the tip. Therefore, the whole electrode does not need to be included in the computational domain, so that a finer spatial discretization can be used. Even then it is hard to resolve the electric field around a sharp tip accurately, as it increases rapidly like $1/r$ or even $1/r^2$ (with r the distance to the tip).

Because of the problems with the charge simulation method, discussed in section IV A, it is difficult to give a quantitative analysis of the error in the electric field. We typically use 10 line charges to represent the electrode surface, which gives a maximum error of a few percent in the potential at the control points. Using more charges reduces this error, but can lead to (very) nonphysical charge configurations in the presence of space charge. This is also the reason why we work with such a sharp tip, as a rounder tip is difficult to simulate if there is space charge around it. The equipotential surface at V_{elec} is not necessarily parallel to the electrode surface even if the error at the control points is zero, and a small error in the potential can lead to a large error in the electric field close to the electrode. This is in itself not too troublesome for our simulations: basically, we just have an electrode with a slightly different shape, which will have a small effect at later stages of the discharge (because the electrode becomes shielded by space charge).

More problematic is that changes in the space charge surrounding the electrode can lead to nonphysical effects on the electrode, as the charge configuration on the axis is determined by the least squares solution of a linear system. It is hard to predict for which configurations this will lead to problematic behavior. Typically, there will be one or more sudden large changes in electric field when space charge starts to build up at the electrode tip, but at later stages the behavior is quite stable.

It needs to be investigated what kind of oscillations would be present in a real electrode when space charge builds up next to it in a few nanoseconds.

B. Swarm experiments

Plasma models are often tested by comparing the swarm parameters generated by simulations to those experimentally measured or obtained before. An electron swarm consists of a number of electrons in a neutral gas of much higher density. For moderate, homogeneous electric fields, the electrons will relax due to the various collisions so that the energy distribution function will depend only on the electric field. Then the swarm can be characterized by so-called swarm parameters, describing the ionization rate, drift velocity, mean energy, diffusion coefficient etc. A historic and a more recent overview of the use of swarm data can be found in [40, 41].

We follow the procedure described in [17] to obtain the swarm parameters from our model, by simulating swarms of electrons starting at the same position in a constant electric field of magnitude E (without space charge effects or photoionization). Initially the electrons relax to the electric field, until at a time t_1 the mean energy is mostly fluctuating due to the finite number of particles in the swarm. Then the simulation runs until the number of particles $N(t)$ is either larger than $\gamma N(t_1)$ or smaller than $N(t_1)/\gamma$, with γ some constant (we use 2.0). The mobility coefficient $\mu(E)$, the effective ionization coefficient $\alpha_{\text{eff}}(E)$ and the diffusion coefficient $D_{x_i}(E)$ along a coordinate x_i can now be approximated by

$$\mu(E) \approx \langle v \rangle / E \tag{16}$$

$$\alpha_{\text{eff}}(E) \approx \frac{1}{\mu(E)E} \frac{\ln\left[N(t_2)/N(t_1)\right]}{t_2 - t_1}, \tag{17}$$

$$D_{x_i}(E) \approx \frac{1}{2} \frac{\left(\langle x_i(t_2)^2 \rangle - \langle x_i(t_2) \rangle^2\right) - \left(\langle x_i(t_1)^2 \rangle - \langle x_i(t_1) \rangle^2\right)}{t_2 - t_1}, \tag{18}$$

where brackets denote the mean over all the electrons, v is the velocity and x_i a Cartesian coordinate. Note that $\mu(E)$ and $\alpha_{\text{eff}}(E)$ are the 'flux coefficients' as discussed in [17], that describe the transport of individual electrons. To describe the evolution of the swarm as a whole, 'bulk coefficients' are used, as is done here for $D_{x_i}(E)$. To illustrate the difference, consider the 'bulk' mean velocity of the swarm, given by

$$\bar{\mathbf{v}}_{\text{bulk}}(t) \approx \frac{\langle \mathbf{x}(t + \Delta t) \rangle - \langle \mathbf{x}(t - \Delta t) \rangle}{2\Delta t}, \tag{19}$$

which is not equal to the 'flux' mean velocity if the number of particles changes

$$\bar{\mathbf{v}}_{\text{flux}}(t) = \langle \mathbf{v}(t) \rangle. \tag{20}$$

By repeating the above procedure for several simulated swarms, one can get an estimate of the variance in the swarm parameters, and we simulate until the relative variance of the mean is smaller than some threshold. We adjust the initial swarm size adaptively (in high fields it becomes smaller, because in the time it takes the electrons to relax, the swarm already grows by a large factor). See figure 6 for the resulting swarm parameters for different electric fields and a comparison with BOLSIG+, which uses isotropic scattering and a different ionization model, where the energy is equally shared between incident and new electron. If these assumptions are used in our particle code, the resulting swarm parameters are nearly identical to the ones generated by BOLSIG+, except for the diffusion constant. The difference could be caused by a different definition of this constant in BOLSIG+, as it uses a two-term spherical harmonics expansion in which (18) cannot directly be measured.

When anisotropic scattering and Opal's formula (11) for the energy sharing are used, the swarm parameters change very little for electric fields below 10 MV/m, since at low energy the scattering is almost isotropic and the energy sharing approximately equal. For higher electric fields there is an increasing difference, although still small at 25 MV/m. (A more general comparison between PIC-MCC codes and BOLSIG+ like solvers can for example be found in [42]).

C. Avalanche statistics

An accurate description of the electron avalanches that grow towards the positive electrode is essential for understanding the inception process. The following integral is often used to estimate the size of an initial avalanche, see for example [43]:

$$S_e(z) = S_e(z_1) \exp\left[\int_{z_1}^{z} \alpha_{\text{eff}}(z')dz'\right], \tag{21}$$

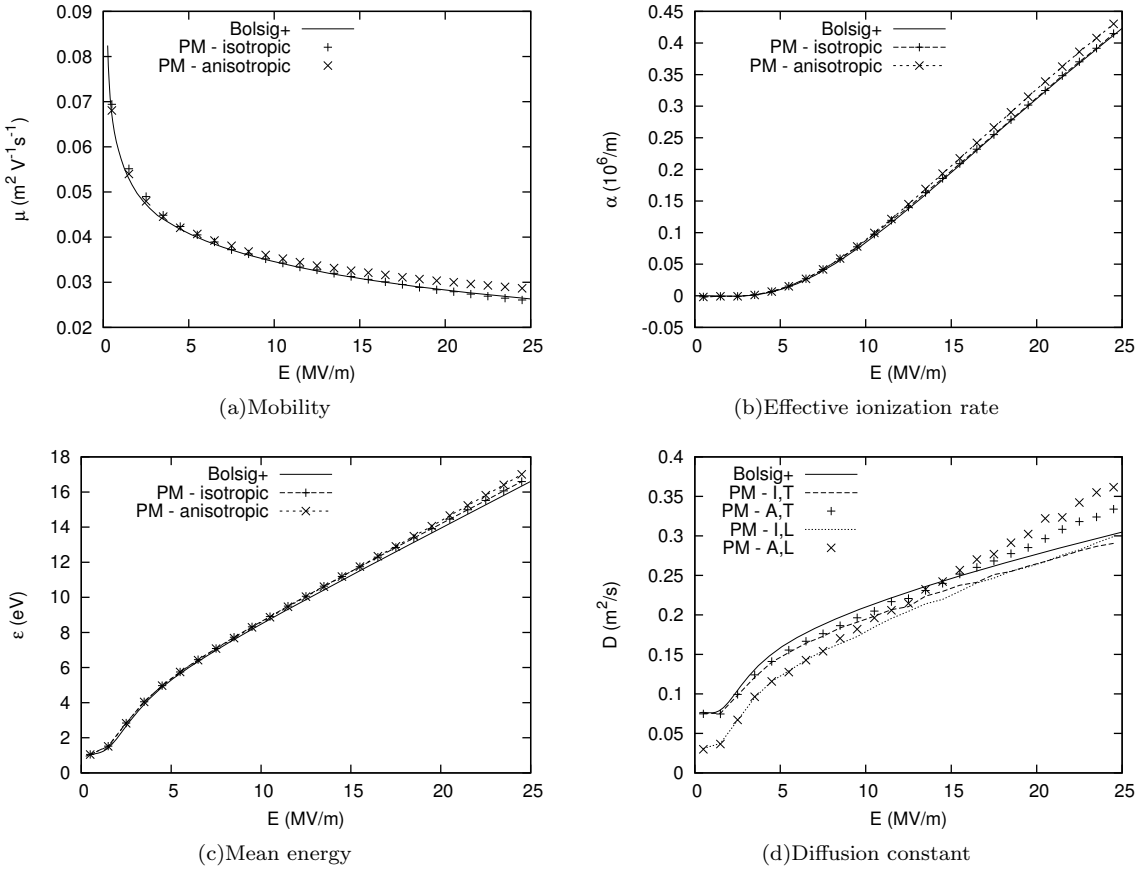

(a)Mobility (b)Effective ionization rate

(c)Mean energy (d)Diffusion constant

FIG. 6: A comparison between the swarm parameters computed by BOLSIG+ and our particle model (PM), in air at 293 K and 1 bar. The label 'isotropic' means that isotropic scattering and equal energy sharing for ionizations was used (like in BOLSIG+), while anisotropic refers to the model described in section IV C. For the diffusion T refers to transversal diffusion (with respect to the electric field), L to longitudinal diffusion, I to isotropic scattering and A to anisotropic scattering.

where $S_e(z)$ is the number of electrons in the avalanche, z is the coordinate along the path of the avalanche and $\alpha_{\text{eff}}(z) = \alpha(z) - \eta(z)$ is the effective bulk ionization coefficient, given by the ionization coefficient $\alpha(z)$ minus the attachment coefficient $\eta(z)$.

Equation (21) is valid under swarm conditions (no space charge and relaxation of electrons to the electric field), with the electric field varying only in the z-direction and no diffusion. Furthermore the number of electrons should be large so that $S_e(z)$ is approximately continuous and stochastic fluctuations are small. Hence (21) has to be interpreted in the following way: if the avalanche starts from some seed at z_0, then it grows stochastically up to z_1, after which the growth can be approximated by (21). Because z_1 and $S_e(z_1)$ are unknown, as well as their distribution, this seems to be of little use. However, the mean avalanche size can be determined, and is given by

$$\bar{S}_e(z) = \exp\left[\int_{z_0}^{z} \alpha_{\text{eff}}(z')dz'\right]. \tag{22}$$

The size distribution of electron avalanches has mostly been studied for the electric fields found in proportional counters, see for example [44, 45]. For weak, uniform electric fields without attachment the distribution is approximately exponential with a relative variance of one:

$$\Pr\left[X = S_e(z)/\bar{S}_e(z)\right] = X \cdot \exp\left(-X\right), \tag{23}$$

For stronger electric fields the distribution will generally have a different shape, which has been approximated by the Polya distribution, i.e.,

$$\Pr\left[X = S_e(z)/\bar{S}_e(z)\right] = \left[m^m/\Gamma(m)\right] X^{m-1} \cdot \exp(-mX), \tag{24}$$

where m typically is 3/2 (with no direct physical meaning). Other distributions have also been used, see [44].

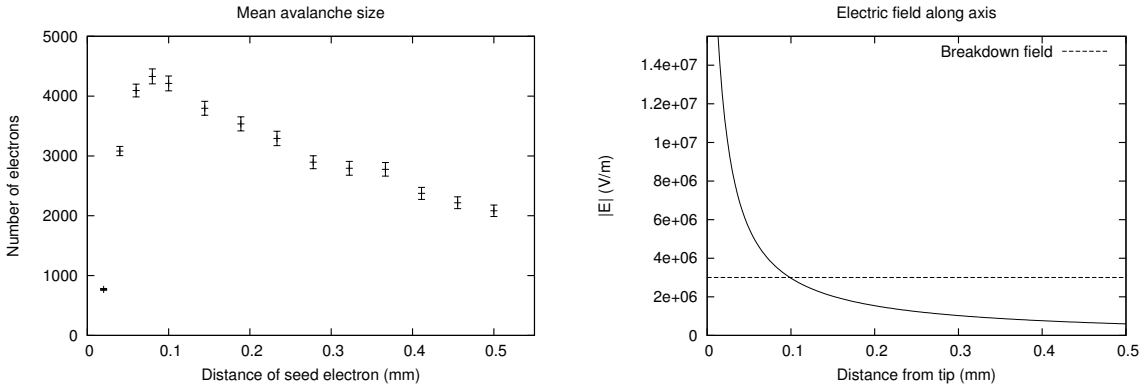

(a) (b)

FIG. 7: (a) The mean avalanche size is shown for a single seed electron released a distance d above the electrode. The mean is taken over 1000 avalanches, with an electrode voltage of +2.0 kV. The error bars indicate one standard deviation. (b) The electric field above the electrode tip.

It is not clear how accurate these approximations are in the geometry we study, because the electric field strongly varies and attachment is important further away from the electrode. Therefore, we have implemented a simple program that repeatedly injects a seed in a 'clean' domain (without charge from previous runs) and then measures the size of the resulting avalanche, so without photoionization to generate new avalanches. We assume that the effect of space charge is negligible, so that the electric field has to be computed only once.

As a first test we release seed electrons above the electrode tip on the axis of symmetry, at various distances d. Figure 7 shows the mean avalanche size versus the distance. When the seed is released very close to the electrode, the avalanche cannot grow very large before it is absorbed, and when the seed is very far from the electrode, there is a large probability of attachment before the avalanche starts to grow. This distribution of avalanche sizes thus looks quite different depending on the distance at which the seed is released, and is shown for three distances in figure 8, where also the corresponding Polya distributions (24) are shown. Although the physical basis for the use of the Polya distribution has been disputed, see for example [46], it matches our results reasonably well.

By taking the derivative of (21) one gets

$$\frac{dS_e(z)}{dz} = \alpha_{\text{eff}}(z), \tag{25}$$

which can be used to find $\alpha_{\text{eff}}(z)$ if $S_e(z)$ is known. To compare the results of our avalanche simulations with (25), we first estimate the mean avalanche size as it moves towards the electrode. We define the avalanche size at some point z' along its path as the integrated flux of electrons passing through z', i.e., the number ionizations minus the number of attachments that occurred at $z < z'$. Since the electric field along the path is known, we can then use (25) to get the ionization rate $\alpha_{\text{fit}}(E)$ that fits the simulation results (although diffusion makes the notion of a one-dimensional path for an avalanche somewhat inaccurate). See figure 9(a) where $\alpha_{\text{fit}}(E)$ is shown together with the ionization coefficients derived from swarm experiments. For an electric field up to $1.3 \cdot 10^7$ V/m, we see that α_{fit} is approximately equal to the bulk effective ionization coefficient, but for higher electric fields it becomes larger, and eventually also larger than the flux ionization coefficient. This is probably because the electrons do not relax to the electric field if it has a large gradient.

The above referred to experiments where the seed electron was released at a certain distance above the electrode tip. When the seed is released at a random position a distance d from the electrode tip, the avalanches are significantly smaller, see figure 9(b).

D. The initiation cloud and streamer formation

If we want to simulate the inception process, we include photoionization and start the simulation with some initial electrons close to the electrode. Due to the axial symmetry of the charge simulation method that we implemented, the space charge close to the electrode should also build up approximately axially symmetric, or else the method becomes unstable. Therefore, we distribute 10^3 electrons as a Gaussian cloud with a standard deviation of 12 μm, on the electrode axis. The electrons will accelerate towards the electrode, increasing their energy, which they lose again due

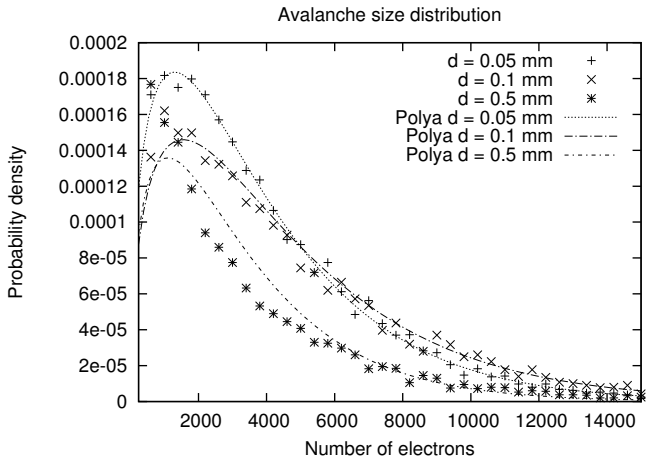

FIG. 8: The avalanche size distribution for seed electrons starting at various distances d from the electrode. The graph is generated from data of 10^4 avalanches, with an electrode voltage of +2.0 kV. Not shown are avalanches of size zero, where the initial electron is attached before any ionization takes place. This happened in 38%, 6.4% and 1.8% of the simulations for $d = 0.5$, 0.1 and 0.05 mm, respectively, with the corresponding mean of the distribution $2.03 \cdot 10^3$, $4.4 \cdot 10^3$ and $3.8 \cdot 10^3$. The lines are Polya distributions as in (24), with the mean taken only over avalanches of size greater than zero.

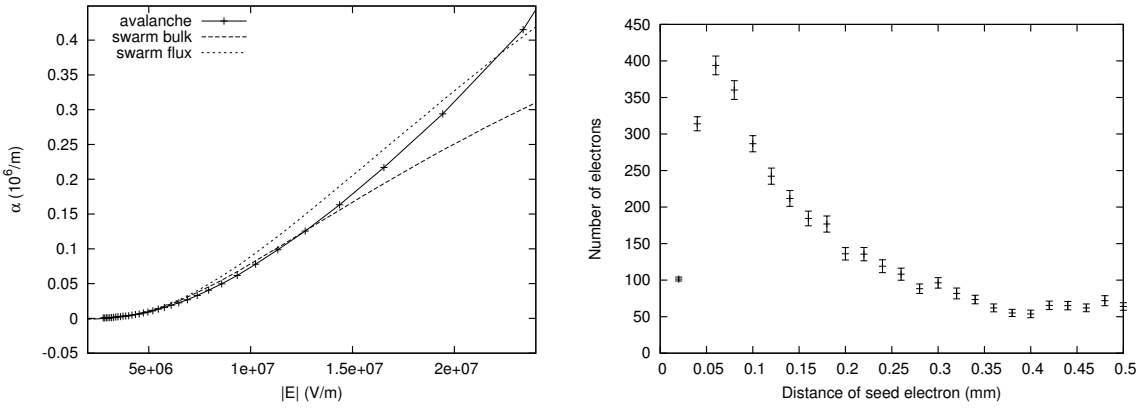

(a) (b)

FIG. 9: (a) The effective ionization coefficient for avalanches moving to the electrode, as defined by (25), for an electrode voltage of +2 kV. Also shown are the flux and bulk effective ionization coefficients obtained from swarm experiments. (b) The mean avalanche size for electrons released at a random location a distance d from the electrode tip, with the electrode at +2 kV. Each data point is generated using 1000 avalanches, and the error bars indicate one standard deviation

to inelastic collisions and ionizations. We have observed three different scenarios depending on the electrode voltage: if it is rather low, the available electrons do not generate enough photoionization events and after some time there are no more electrons left. If the voltage is increased, sometimes an almost steady state can be reached (at least up to the order of nanoseconds), where a small region above the tip of the electrode remains ionized, but does not grow. This can be explained by the fact that the space charge shields the sharp electrode tip, reducing the electric field and preventing further growth. When the voltage is increased further, this ionized region grows to a larger size and will eventually destabilize into on or more streamers.

These three scenarios compare well to experimental observations, however, the voltages at which they occur seem to be slightly different, as will be discussed in section V E. Another similarity is that in experiments often a small glowing dot is observed at the electrode tip, see figure 10. In the simulations we observe that the electron and ion density in front of the tip is much larger than in other regions. At some point this causes an instability, because the plasma oscillations can no longer be resolved accurately (these oscillations arise if the electrons are slightly displaced with respect to the ions, because there will be a restoring Coulomb force). For example, if the electron density is

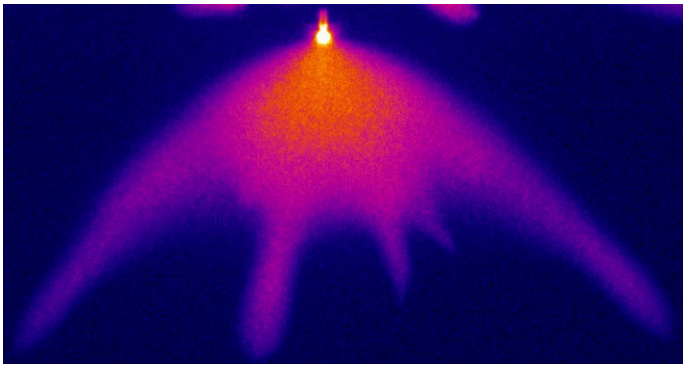

FIG. 10: A recorded image of a discharge in N_2 at 100 mbar, where an initiation cloud has just destabilized into several streamers (image by S. Nijdam, personal communication). The small cylinder at the top is the electrode, and a very bright spot is visible just below the electrode tip, where the electron and ion density is very high. The same phenomenon in air causes problems in our simulations, see the text.

$n_e = 10^{22}/\mathrm{m}^3$, then the plasma frequency is

$$f_{\mathrm{pe}} = \frac{1}{2\pi}\sqrt{\frac{n_e e^2}{m_e \epsilon_0}} \approx 10^{12}\ \mathrm{Hz}, \tag{26}$$

which can only be resolved by using a timestep at least an order of magnitude smaller than $1/f_{\mathrm{pe}}$. Even then an instability could grow, as the large amount of space charge present causes small errors to lead to high electric fields. This effect does not play a role in other parts of the domain because the electron and ion density are both much lower and smoother there, so the electric field caused by such oscillations would be negligible compared to the background electric field. As these instabilities at the tip are not of our primary interest for the later development of the discharge, we artificially limit the electric field in regions of high electron density. If the electron density is higher than $n_c = 5 \cdot 10^{20}\ \mathrm{m}^{-3}$ then the electric field E gets limited to

$$E_{\mathrm{lim}} = \min\left[E,\ E_{\mathrm{max}}/\left(E\,\kappa\,\frac{n_c}{n_e}\right)\right], \tag{27}$$

where $E_{\mathrm{max}} = 5.0 \cdot 10^7\ \mathrm{V/m}$ and $\kappa = \min\left[1.0,\ N_e/(3 \cdot 10^9)\right]$ with N_e the total number of electrons in the simulation. The inclusion of the κ term is to not reduce the electric field in the beginning of the discharge. The physical argument for this procedure is that these regions are more or less conducting, so that the electric field should not become too large. It does however lead to some artifacts, for example the high electric fields next to the electrode tip in figure 12(c), and a different method should be used in the future.

In figure 11 we present the evolution of the electron density for varying photoionization efficiencies. Initially there are 10^3 electron-ion pairs about $80\,\mu$m above the electrode, distributed as a Gaussian cloud with a standard deviation of 12μm. The rescaling algorithm is set to keep at least 128 particles in a cell, and the domain consists of 128^3 cells of volume $(12\mu\mathrm{m})^3$.

In figure 12 the charge density, mean energy, potential and electric field are shown at $t = 2.8$ ns by taking a slice through the center of the domain. Close to the electrode there is an alternating positive and negative charge density, which is most likely related to the plasma oscillations discussed above. The electric field and mean energy are clearly correlated, and we see that a higher photoionization efficiency leads to more rounded shapes and thus lower electric fields and energies. In the electric potential one can recognize the line charges of the charge simulation method. Problems with this method probably cause the potential in the inception cloud to rise significantly above V_{elec}, and we see that the inception cloud itself is almost equipotential.

We can try to understand the growth and destabilization of the initiation cloud in the following way. The growth of the ionized region in a certain direction depends mostly on the strength of the electric field (which should point inwards), but there need to be seed electrons ahead from which avalanches can grow. In the beginning of the discharge the growth is mostly governed by the electric field distribution from the electrode, as ionizations predominantly take place in the region of highest electric field. This is why the initial initiation clouds look similar. When the space charge starts to 'shield' the field from the electrode, the growth becomes more dependent on the present space charge distribution (that influences the electric field) and the availability of electrons outside. With a low photoionization efficiency this quickly leads to the formation of irregular structures. But also with more photoionization the initiation

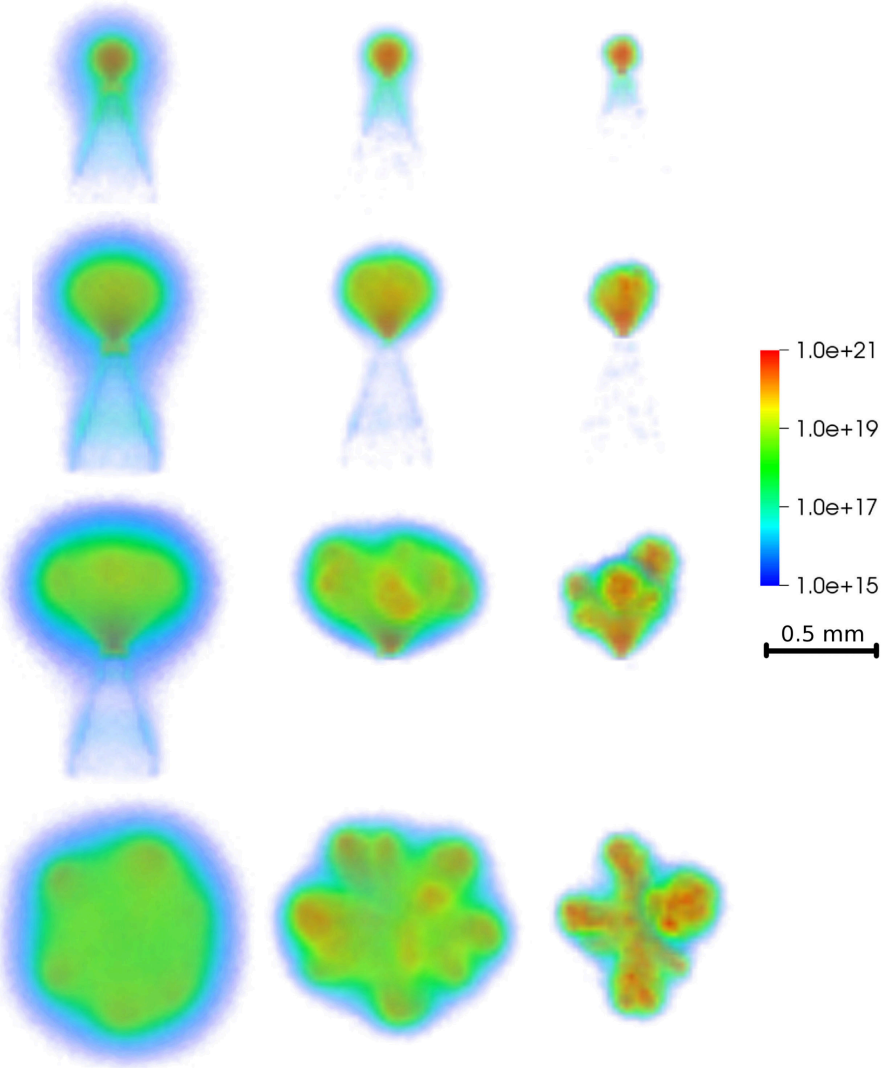

FIG. 11: The electron density per m^3 around a +4.0 kV electrode, shown with logarithmic color scale. Time runs from top to bottom as $t = 0.5,\ 1.5,\ 2.5$ and 2.8 ns, and the bottom row is shown in top view. The photoionization efficiency is reduced by a factor of 10 in the middle column and by a factor of 100 in the right column.

cloud will eventually destabilize, because a small perturbation can locally enhance the electric field and thus grow larger.

The photoionization efficiency has a remarkably strong effect on the simulations. Less photoionization seems to lead to thinner structures and more branches, in agreement with [27, 47]. This can directly be used to test the modified Zheleznyak model of section IV E, by comparing simulation results with experiments. See also figure 13, which shows experimental observations of streamer inception in air and in N_2 of purity 6.0 (less than 1 ppm oxygen), at various pressures. Reducing the amount of oxygen increases the absorption length of the photons, thereby reducing the amount of photoionization close to the discharge. This leads to the formation of thinner structures with more branches, like in the simulations.

E. Inception voltage and probability

In discharge experiments there is usually a well-defined inception or critical voltage V_c, the lowest voltage at which inception starts to occur, that depends on the electrode geometry and experimental conditions like gas composition or pressure. Often a pulsed voltage source is used to study streamer inception and then it is observed that not every pulse above the critical voltage for inception leads to a visible discharge. See for example [48], where a study of the

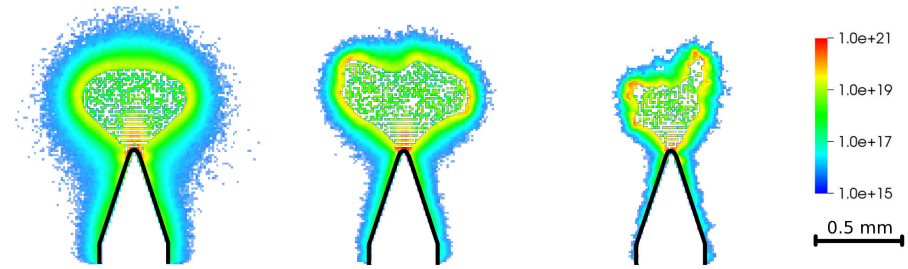

(a)The (positive) charge density at the cell centers, in e/m^3.

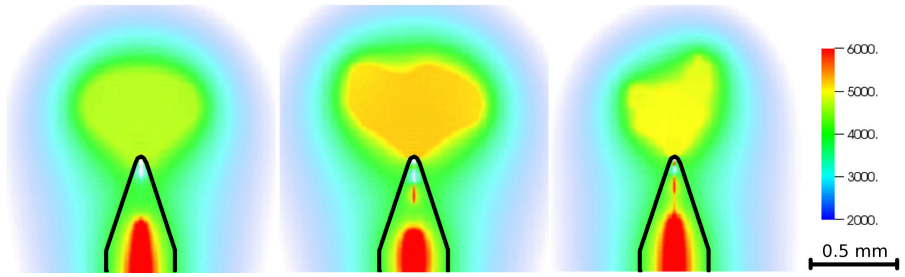

(b)The electric potential in Volt.

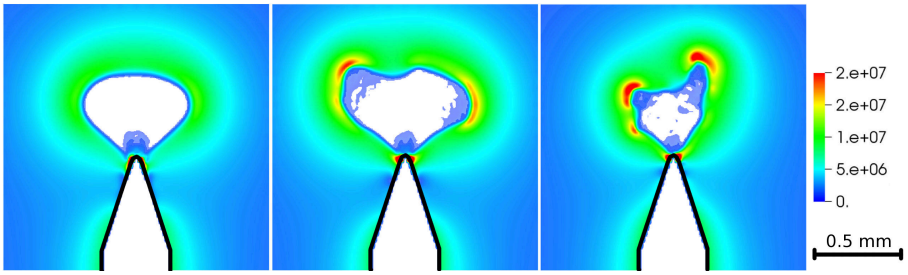

(c)The electric field strength in V/m.

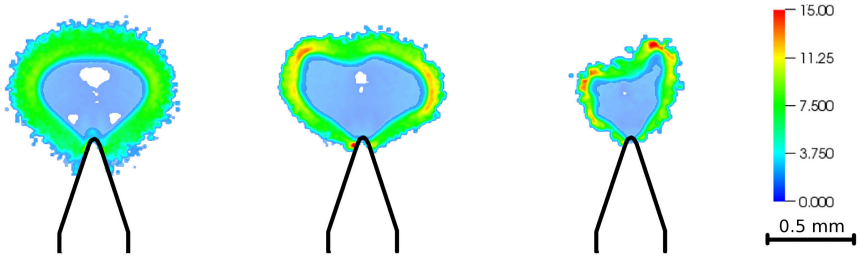

(d)The mean energy in eV.

FIG. 12: Slices through the middle of the domain at $t = 2.8$ ns (see figure 11). The photoionization efficiency is reduced by a factor of 10 in the middle column and by a factor of 100 in the right column.

inception behavior of positive streamers in different gases was performed.

We have not yet performed such a study, but we expect that the probability of streamer inception will roughly depend on four factors: the availability of free electrons that create the initial electron avalanches, the typical size of these initial avalanches, the efficiency with which new free electrons are generated to form consecutive avalanches and the effect of space charge on the electrode (e.g., the electric field of a sharp electrode can be reduced by space charge, while the field of a round electrode can be increased).

Sources of free electrons have been discussed in [35], and in particular the effect of background ionization was recently experimentally investigated in [27]. In future work the process of electron detachment from O_2^- could be included in our simulation, together with a realistic background ionization level, to compare the inception probability in simulation and experiment.

The critical voltage does not depend on the background ionization level, so we can make a first qualitative comparison with experiments. In [48] an electrode was used with a tip radius of 15 μm, which is comparable to our simulated

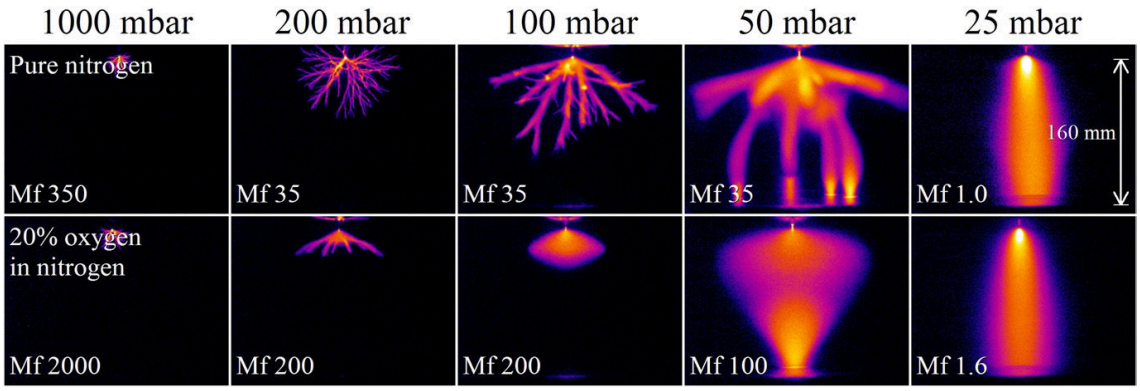

FIG. 13: Picture taken from [27], showing discharges in air and in N_2 of purity 6.0 at various pressures. In pure N_2 there is less photoionization close to the discharge and we observe thinner structures with more branches, like in our simulations.

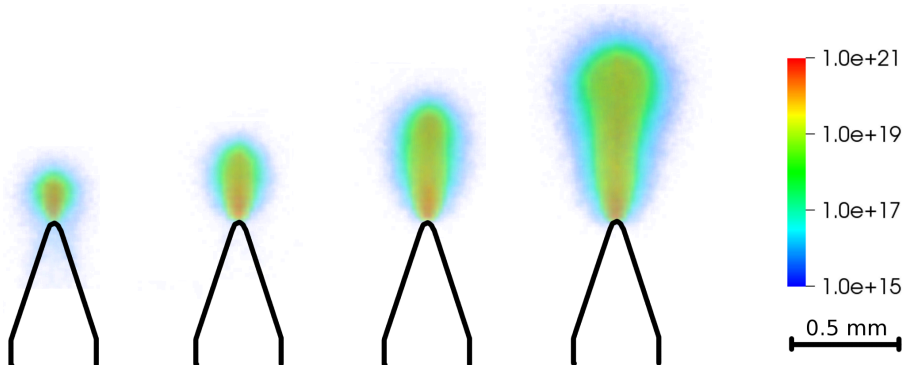

FIG. 14: The electron density per m^3 around a +2.5 kV electrode, shown with logarithmic color scale. Time runs as t = 2, 4, 6, 8 ns from left to right. Because the initiation cloud is small it can quickly destabilize into a single streamer.

electrode which has a radius of curvature of 24 μm. For different voltages they generated 100 pulses with a rise time of 20 ns, and they started to see 'streamer inception' between 4 and 6 kV in ambient air, although it is not clear what qualifies as streamer inception. In similar measurements [49] streamers with a length of about 5 mm were observed at 5 kV. In our simulations we observe a small initiation cloud with a voltage as low as 2.25 kV, that more or less stabilizes (at least up to 10 ns). At 2.5 kV we have seen a single streamer develop from the inception cloud, see figure 14. However, the conditions we use are quite different: we start with a Gaussian cloud of 10^3 electrons close to the electrode, we include no rise-time for the electrode voltage and we can only observe streamers of less than a millimeter in length. The formation of multiple streamers from the initiation cloud requires a higher voltage, probably close to 4 kV considering the faint emergence of streamers in figure 15. For a more quantitative comparison with experiments it would probably be best to first implement the electrode in a more accurate and robust way. Then differences could be related to, for example, the cross sections used or the photoionization efficiency.

In literature on the inception voltage of corona discharges [35, 50, 51] it is often assumed that only electrons close to the electrode, where the field is above the breakdown value, will generate an avalanche, of a size given by (22). From figures 7–9 we see that this is a rather crude assumption. The effect of space charge on the electric field around the electrode should also be considered, because the streamers only emerge when the initiation cloud destabilizes (at which point there must be significant space charge).

F. The effect of super-particles

When super-particles are used this increases the stochastic fluctuations due to the finite number of particles. To get a rough estimate of this effect, consider some quantity X that is the sum of N independent samples z_i, and another

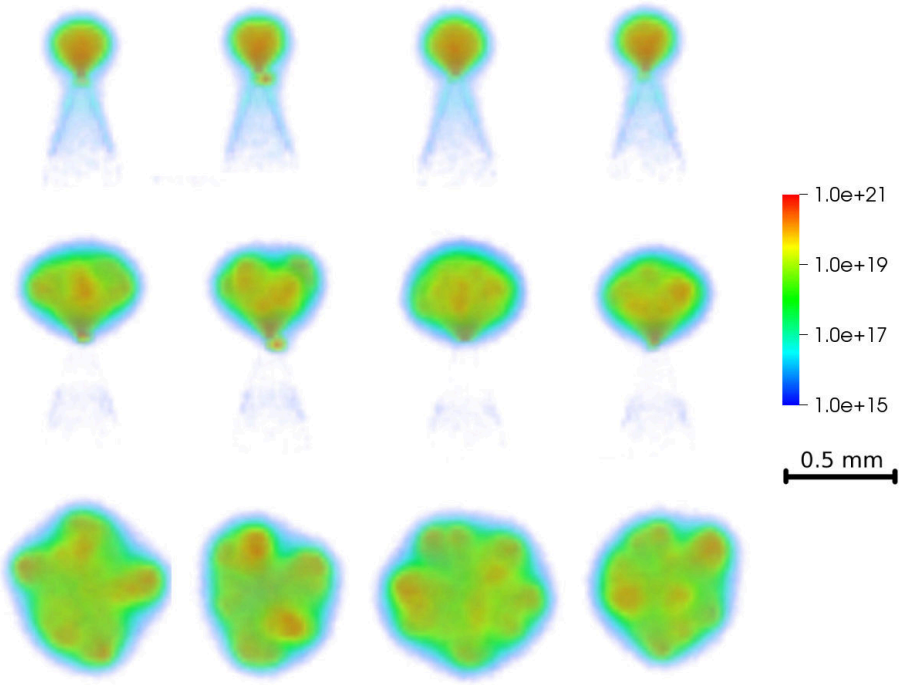

FIG. 15: The electron density per m^3 around a +4 kV electrode, at $t = 1.0$ ns (top row), $t = 2.0$ ns (middle row) and $t = 2.5$ ns (bottom row, top view). The minimum number of particles in a cell for the rescaling algorithm is varied from left to right as $M_{\min} = 32, 64, 128, 256$. Note that the color scale is logarithmic.

quantity Y that is the sum of N/β samples $\beta \cdot z_i$. Then it follows that

$$\mathrm{Var}(Y) = \beta \cdot \mathrm{Var}(X), \quad \mathrm{Var}\left(\frac{Y}{N/\beta}\right) = \beta^3 \cdot \mathrm{Var}\left(\frac{X}{N}\right). \tag{28}$$

So if we have super-particles with mean weight β, the stochastic fluctuations of the charge density in some region for example increase roughly proportional to $\sqrt{\beta}$ (note that the samples are not truly independent here).

The use of super-particles leads to so-called numerical heating, where the kinetic energy of particles increases during the simulation due to non-physical effects. For example, the electric field in the streamer channel is usually very weak, but if only a few particles are used to describe the charge density there, then the fluctuations in electric field will give them a higher energy. The concept of numerical heating is described in some detail in [14, 52, 53], although these texts are about quite different types of simulations. In our simulations particles lose their energy quite quickly and we are more interested in streamer-related parameters than in an increase of the mean energy.

In our simulation we can vary the minimum number of particles that must be present in a cell in order to form new super-particles, with the parameter $M_{\min}$. We have performed a series of simulations with the same starting conditions, but different values of $M_{\min} = 32, 64, 128, 256$, see figure 15 (a higher value should be more accurate). To show possible differences in the destabilization more clearly, the photoionization efficiency (see figure 4) was decreased by a factor of ten, and in all cases a maximum super-particle weight of 10^4 was used. Although the evolution is different in each case, the correlation with $M_{\min}$ is rather weak. In figure 16 the number of real electrons and super-particles is shown over time. The number of electrons is again weakly correlated to $M_{\min}$, but the number of particles over time, of course, is. In all cases the electric field at the inner parts of the initiation cloud is about $E_{\text{breakdown}}/15$. These results suggest that the rescaling algorithm works rather well, and more in general that adaptive super-particle creation is a viable method for such simulations. The essential property of our rescaling algorithm seems to be that it does not create super-particles in regions of low electron density. The fluctuations in these regions are therefore well resolved and seem to be the most important for the development of the discharge, see also [17, 54].

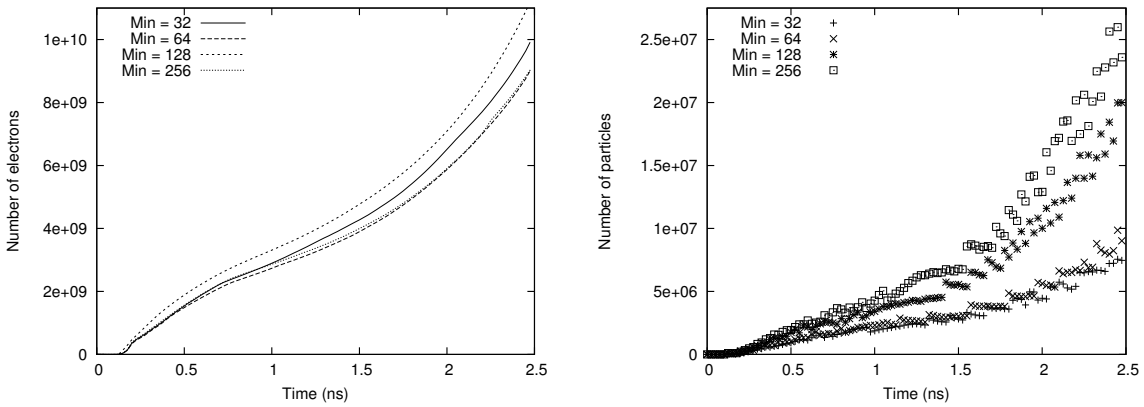

FIG. 16: The number of real electrons (left) and the number of super-particles (right) over time, for a varying minimum number of particles in a cell $M_{\min} = 32$, 64, 128, 256. The electrode voltage is +4 kV and the photoionization efficiency is reduced by a factor of 10.

VI. FUTURE IMPROVEMENTS

Important improvements could be made in the computation of the electric field and the inclusion of an electrode, as was already discussed in section IV A. The current approach with a fast elliptic solver (FISHPACK) and the charge simulation method is quite fast, but has several downsides: the electrode undergoes nonphysical transitions when the space charge builds up, its shape cannot be resolved accurately, its tip has to be very sharp, which limits the possibilities of a quantitative comparison with experiment, and the discharge can only start from axial symmetry. These problems could be resolved by using a more flexible solver for the Poisson equation, for example a multigrid method that can work with embedded boundaries and adaptive mesh refinement, and that ideally can run in parallel. Such a solver seems to be included in CHOMBO package [55], and for future work we will investigate whether it is fast and flexible enough for use in 3D discharge simulations. The influence of the mesh resolution on the destabilization of the initiation cloud should also be investigated.

Currently, the particle code uses trilinear interpolation to map the particles to charge densities, known as cloud-in-cell or CIC. One can construct interpolation schemes of arbitrary order, see for example [56]. As the order increases the effective particle shape (e.g., a rectangle of width Δx at zeroth order, a triangle with base $2\Delta x$ at first order) approaches a Gaussian function with standard deviation $\Delta x \cdot \sqrt{n/12}$, where n is the order of the interpolation. It could be interesting to use a different interpolation scheme for particles in different regions of the domain or for particles of different weight. Then it would be possible to use 'smoother' particles of very high weight in the streamer channel without creating too much numerical heating, a possible alternative to hybrid modeling.

The rescaling algorithm presented in section IV F seems to work quite well, but only increases the weight of particles. For the simulation of inception near positive electrodes this is reasonable, because electrons typically move to regions of higher electron density in time. However, it could still create artifacts (earlier destabilization of the inception cloud, for example), as some particles of high weight also move to regions of low density, where they can create significant perturbations. Therefore, another improvement could be to include a mechanism for splitting super-particles up again. Such an algorithm can also be useful for the simulation of negative streamers with PIC-MCC methods.

VII. SUMMARY

We have presented a particle based 3D model for the study of streamer inception near positive electrodes. Although the inclusion of the electrode should be improved in the future, the first results look promising and confirm that the adaptive creation of super-particles is a viable strategy for this type of modeling. The simulations show that the stochastic noise of the particle model and the full 3D approach are essential for the study of the inception process. In the future the model could be used for quantitative comparisons with experiments, and we have already observed a strong effect of the photoionization efficiency: a higher number of photo-electrons leads to smoother structures, thicker streamer channels and thus lower electric fields. We have also presented data on the statistics of initial electron avalanches, an important first step in the understanding of the inception voltage and probability.

Acknowledgments

I would hereby like to thank Ute Ebert for letting me do my master project in the productive and friendly environment that her group and CWI provide, and for the opportunities that I have gotten to meet new people and expand my knowledge. I would also like to thank Chao Li and Sander Nijdam for their help.

---

[1] T. Yamamoto, K. Ramanathan, P.A. Lawless, D.S. Ensor, J.R. Newsome, N. Plaks, and G.H. Ramsey. Control of volatile organic compounds by an ac energized ferroelectric pellet reactor and a pulsed corona reactor. *Industry Applications, IEEE Transactions on*, 28(3):528 –534, 1992.

[2] E J M van Heesch, G J J Winands, and A J M Pemen. Evaluation of pulsed streamer corona experiments to determine the O* radical yield. *Journal of Physics D: Applied Physics*, 41(23):234015, 2008.

[3] Gregory Fridman, Gary Friedman, Alexander Gutsol, Anatoly B. Shekhter, Victor N. Vasilets, and Alexander Fridman. Applied Plasma Medicine. *Plasma Processes and Polymers*, 5(6):503–533, 2008.

[4] S.A. Nair, A.J.M. Pemen, K. Yan, F.M. van Gompel, H.E.M. van Leuken, E.J.M. van Heesch, K.J. Ptasinski, and A.A.H. Drinkenburg. Tar removal from biomass-derived fuel gas by pulsed corona discharges. *Fuel Processing Technology*, 84(1-3):161 – 173, 2003.

[5] Sander Nijdam. *Experimental investigations on the physics of streamers*. PhD thesis, Technische Universiteit Eindhoven, 2011.

[6] C V Nguyen, A P J van Deursen, and U Ebert. Multiple x-ray bursts from long discharges in air. *Journal of Physics D: Applied Physics*, 41(23):234012, 2008.

[7] U Ebert, C Montijn, T M P Briels, W Hundsdorfer, B Meulenbroek, A Rocco, and E M van Veldhuizen. The multiscale nature of streamers. *Plasma Sources Science and Technology*, 15(2):S118, 2006.

[8] T.M.P. Briels, E.M. van Veldhuizen, and U. Ebert. Time resolved measurements of streamer inception in air. *Plasma Science, IEEE Transactions on*, 36(4):908 –909, 2008.

[9] T M P Briels, E M van Veldhuizen, and U Ebert. Positive streamers in air and nitrogen of varying density: experiments on similarity laws. *Journal of Physics D: Applied Physics*, 41(23):234008, 2008.

[10] S Nijdam, F M J H van de Wetering, R Blanc, E M van Veldhuizen, and U Ebert. Probing photo-ionization: experiments on positive streamers in pure gases and mixtures. *Journal of Physics D: Applied Physics*, 43(14):145204, 2010.

[11] S. Nijdam, K. Miermans, E. M. van Veldhuizen, and U. Ebert. A peculiar streamer morphology created by a complex voltage pulse. *Plasma Science, IEEE Transactions on*, PP(99):1 –2, 2011.

[12] C.K. Birdsall. Particle-in-cell charged-particle simulations, plus monte carlo collisions with neutral atoms, pic-mcc. *Plasma Science, IEEE Transactions on*, 19(2):65 –85, 1991.

[13] K. Nanbu. Probability theory of electron-molecule, ion-molecule, molecule-molecule, and coulomb collisions for particle modeling of materials processing plasmas and cases. *Plasma Science, IEEE Transactions on*, 28(3):971 –990, 2000.

[14] Charles K. Birdsall and A. Bruce. Langdon. *Plasma physics via computer simulation / Charles K. Birdsall, A. Bruce Langdon*. McGraw-Hill, New York :, 1985.

[15] A. Luque and U. Ebert. Density models for streamer discharges: Beyond cylindrical symmetry and homogeneous media. *Journal of Computational Physics*, (0):–, 2011.

[16] R D White, R E Robson, S Dujko, P Nicoletopoulos, and B Li. Recent advances in the application of boltzmann equation and fluid equation methods to charged particle transport in non-equilibrium plasmas. *Journal of Physics D: Applied Physics*, 42(19):194001, 2009.

[17] Chao Li, Ute Ebert, and Willem Hundsdorfer. Spatially hybrid computations for streamer discharges: II. Fully 3D simulations. *Journal of Computational Physics*, (0):–, 2011.

[18] R. W. Hockney and J. W. Eastwood. *Computer simulation using particles*. IOP Publishing Ltd., Bristol, England, 1988.

[19] Hans Johansen and Phillip Colella. A cartesian grid embedded boundary method for poisson's equation on irregular domains. *J. Comput. Phys.*, 147:60–85, 1998.

[20] Sebastien Celestin, Zdenek Bonaventura, Barbar Zeghondy, Anne Bourdon, and Pierre Sgur. The use of the ghost fluid method for poisson's equation to simulate streamer propagation in point-to-plane and point-to-point geometries. *Journal of Physics D: Applied Physics*, 42(6):065203, 2009.

[21] Chao Li. *Joining particle and fluid aspects in streamer simulations*. PhD thesis, Technische Universiteit Eindhoven, 2009.

[22] N.H. Malik. A review of the charge simulation method and its applications. *Electrical Insulation, IEEE Transactions on*, 24(1):3 –20, 1989.

[23] J. Adams, P. Swarztrauber, and R. Sweet. Fishpack90, `http://www.cisl.ucar.edu/css/software/fishpack90/`.

[24] Loup Verlet. Computer "experiments" on classical fluids. i. thermodynamical properties of lennard-jones molecules. *Phys. Rev.*, 159:98–103, 1967.

[25] D. Nelson, M. Benhenni, O. Eichwald, and M. Yousfi. Ion swarm data for electrical discharge modeling in air and flue gas mixtures. 94(1):96–103, 2003.

[26] L.C. Pitchford and J.P. Boeuf. The siglo data base, `http://www.lxcat.laplace.univ-tlse.fr`, 2011.

[27] S Nijdam, G Wormeester, E M van Veldhuizen, and U Ebert. Probing background ionization: positive streamers with varying pulse repetition rate and with a radioactive admixture. *Journal of Physics D: Applied Physics*, 44(45):455201,

2011.

[28] O. Chanrion and T. Neubert. A pic-mcc code for simulation of streamer propagation in air. *Journal of Computational Physics*, 227(15):7222 – 7245, 2008.

[29] V. Vahedi and M. Surendra. A monte carlo collision model for the particle-in-cell method: applications to argon and oxygen discharges. *Computer Physics Communications*, 87(1-2):179 – 198, 1995. Particle Simulation Methods.

[30] A. Okhrimovskyy, A. Bogaerts, and R. Gijbels. Electron anisotropic scattering in gases: A formula for monte carlo simulations. *Phys. Rev. E*, 65(3):037402, 2002.

[31] C. B. Opal, W. K. Peterson, and E. C. Beaty. Measurements of secondary electron spectra produced by electron impact ionization of a number of simple gases. 55(8):4100–4106, 1971.

[32] A. V. Phelps and L. C. Pitchford. Anisotropic scattering of electrons by $n2$ and its effect on electron transport. *Phys. Rev. A*, 31(5):2932–2949, 1985.

[33] Ph. Belenguer and L. C. Pitchford. Effect of anisotropy in the elastic scattering cross sections on the ionization source terms in glow discharges in argon. 86(9):4780–4785, 1999.

[34] M. Surendra, D. B. Graves, and G. M. Jellum. Self-consistent model of a direct-current glow discharge: Treatment of fast electrons. *Phys. Rev. A*, 41(2):1112–1125, 1990.

[35] S Pancheshnyi. Role of electronegative gas admixtures in streamer start, propagation and branching phenomena. *Plasma Sources Science and Technology*, 14(4):645, 2005.

[36] M. B. Zhelezniak, A. K. Mnatsakanian, and S. V. Sizykh. Photoionization of nitrogen and oxygen mixtures by radiation from a gas discharge. *Teplofizika Vysokikh Temperatur*, 20:423–428, 1982.

[37] Ningyu Liu and Victor P. Pasko. Effects of photoionization on propagation and branching of positive and negative streamers in sprites. *J. Geophys. Res.*, 109(A4):A04301, 2004.

[38] A. K. Mnatsakanyan, G. V. Naidis, and B. M. Smirnov. Charged particles production and loss processes in nitrogen-oxygen plasmas. *Reviews of Plasma Chemistry*, 1:259 – 292, 1991.

[39] G J M Hagelaar and L C Pitchford. Solving the boltzmann equation to obtain electron transport coefficients and rate coefficients for fluid models. *Plasma Sources Science and Technology*, 14(4):722, 2005.

[40] J. Dutton. A survey of electron swarm data. *Journal of Physical and Chemical Reference Data*, 4(3):577–856, 1975.

[41] Z Lj Petrović, S Dujko, D Marić, G Malović, Nikitović, O aić, J Jovanović, V Stojanović, and M Radmilović-Raenović. Measurement and interpretation of swarm parameters and their application in plasma modelling. *Journal of Physics D: Applied Physics*, 42(19):194002, 2009.

[42] H.C. Kim and J.P. Verboncoeur. Validity of the two-term boltzmann approximation employed in fluid models. In *Plasma Science, 2007. ICOPS 2007. IEEE 34th International Conference on*, page 855, 2007.

[43] A. Pedersen. On the electrical breakdown of gaseous dielectrics-an engineering approach. In *Electrical Insulation and Dielectric Phenomena, 1989. Annual Report., Conference on*, pages 21 –58, 1989.

[44] G. D. Alkhazov. Statistics of electron avalanches and ultimate resolution of proportional counters. *Nuclear Instruments and Methods*, 89:155 – 165, 1970.

[45] J. Byrne. Statistics of electron avalanches in the proportional counter. *Nuclear Instruments and Methods*, 74(2):291 – 296, 1969.

[46] W Legler. The influence of the relaxation of the electron energy distribution on the statistics of electron avalanches. *British Journal of Applied Physics*, 18(9):1275, 1967.

[47] G Wormeester, S Pancheshnyi, A Luque, S Nijdam, and U Ebert. Probing photo-ionization: simulations of positive streamers in varying n 2 : O 2 -mixtures. *Journal of Physics D: Applied Physics*, 43(50):505201, 2010.

[48] E M van Veldhuizen and W R Rutgers. Inception behaviour of pulsed positive corona in several gases. *Journal of Physics D: Applied Physics*, 36(21):2692, 2003.

[49] T M P Briels, J Kos, G J J Winands, E M van Veldhuizen, and U Ebert. Positive and negative streamers in ambient air: measuring diameter, velocity and dissipated energy. *Journal of Physics D: Applied Physics*, 41(23):234004, 2008.

[50] G V Naidis. Conditions for inception of positive corona discharges in air. *Journal of Physics D: Applied Physics*, 38(13):2211, 2005.

[51] Kiyoto Nishijima, Toshiyuki Ishii, and Yasuji Izawa. The statistical inception mechanism of the first corona in positive nonuniform air gaps ranging from 0.3 to 1.0 cm. *Electrical Engineering in Japan*, 158(2):1–8, 2007.

[52] Hiroko Ueda, Yoshiharu Omura, Hiroshi Matsumoto, and Takashi Okuzawa. A study of the numerical heating in electrostatic particle simulations. *Computer Physics Communications*, 79(2):249 – 259, 1994.

[53] Estelle Cormier-Michel, B. A. Shadwick, C. G. R. Geddes, E. Esarey, C. B. Schroeder, and W. P. Leemans. Unphysical kinetic effects in particle-in-cell modeling of laser wakefield accelerators. *Phys. Rev. E*, 78:016404, 2008.

[54] A. Luque and U. Ebert. Electron density fluctuations accelerate the branching of positive streamer discharges in air. *Phys. Rev. E*, 84:046411, 2011.

[55] P. Colella et al. Chombo software package for amr applications, `https://commons.lbl.gov/display/chombo/`.

[56] Hirotade Abe, Natsuhiko Sakairi, Ryohei Itatani, and Hideo Okuda. High-order spline interpolations in the particle simulation. *J. Comput. Phys.*, 63:247–267, 1986.